Final published version of this article: Applied Surface Science, Volume 644, 30 January 2024, 158785
Available online: 1 November 2023
DOI: https://doi.org/10.1016/j.apsusc.2023.158785

Thermal- and Air- Stability of the Compositional Variants of van der Waals Pt-Telluride Thin Films Probed by High Resolution Photoemission Spectroscopy

Vimukthi Pathirage,[1] Nirosha Ravinath Rajapakse,[1] Kinga Lasek,[1] Igor Píš,[2] Federica Bondino,[2] Matthias Batzill[1,#]

[1] Department of Physics, University of South Florida, Tampa, FL 33620, USA

[2] CNR-IOM, Istituto Officina dei Materiali, AREA Science Park, 34149 Basovizza, Trieste, Italy

[#] corresponding author: mbatzill@usf.edu

Abstract:

The Pt-Te compositional phase diagram consists of at least three different compositional line phases ($PtTe_2$, Pt_3Te_4, and Pt_2Te_2) that can be described as layered van der Waals materials. This presents challenges in controlling the composition of ultrathin Pt-telluride 2D materials by physical vapor deposition methods. Here we show by temperature programmed synchrotron photoemission spectroscopy that the different phases have varying thermal stability in vacuum. This enables the synthesis of these materials by preparation of $PtTe_2$ films at low growth temperatures and subsequent vacuum annealing to ~ 350 ˚C for Pt_3Te_4, or ~400 ˚C for Pt_2Te_2. Such prepared phases are characterized by high resolution core level spectroscopy to provide reference spectra for these materials. Moreover, the chemical stability of these materials was tested by exposure to oxygen and air. Even after prolonged air exposure only the surface Te layer was modified by oxygen chemical bonds that caused a 3-eV shift to higher binding energy of the Te-3d core levels. However, these oxygen species could be desorbed by vacuum annealing at 280 ˚C and pristine Pt-telluride samples can be re-established. This shows the excellent chemical stability of these materials, important for practical applications.

I. Introduction

The Pt-Te phase diagram consists of layered van der Waals materials with different compositions.[1,2,3,4] On the tellurium rich side is the Pt-ditelluride with a 1T phase (octahedral coordination of Pt-atoms) and on the Te-poor side is the Pt-monotelluride phase. In between, the Pt_3Te_4 phase consists of alternating van der Waals layers of Pt-ditelluride and Pt-monotelluride. The latter also occurs naturally as the recently discovered mineral, named Mitrofanovite.[5] Schematic illustrations of these three Pt-Te van der Waals materials are shown in Figure 1. $PtTe_2$ and Pt_3Te_4 have been experimentally studied for their electrocatalytic hydrogen evolution reaction[6,7,8] and particularly Pt_3Te_4 has shown very promising onset potentials and Tafel slopes, coming close to those of pure Pt.[9] Pt-monotelluride has not been experimentally studied so far, but a theoretical investigation suggests that the monolayer may possess promising oxygen reduction reaction properties.[10] In addition to the electrocatalytic properties, the $PtTe_2$ and Pt_3Te_4 crystals have attracted attention due to topologically protected Dirac cones in their electronic band structures.[11,12,13,14]

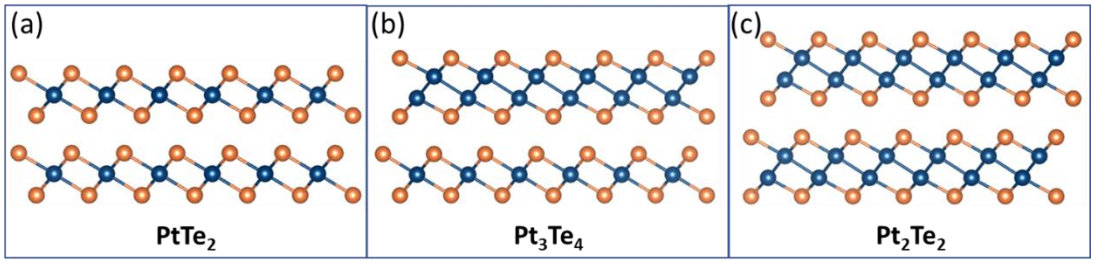

Figure 1: Cross-sectional ball-and-stick models of three van der Waals materials (a) $PtTe_2$, (b) Pt_3Te_4- alternating layers of $PtTe_2$ and Pt_2Te_2, and (c) Pt_2Te_2.

The exciting properties and potential diverse applications of these materials require a better understanding of their synthesis as thin films with controlled stoichiometry and their chemical stability to air exposure. It has been shown that Pt telluride films can be grown on different substrates.[15,16,17,18] Also vacuum annealing results in loss of Te and transformation into Te-poor phases.[19,20] Compositional changes by vacuum annealing can provide a reliable approach for the synthesis of different phases, if those phases exhibit distinct thermal stabilities. To accurately determine transformation temperature and phase stability ranges temperature programmed photoemission spectroscopy is being used here and thus giving insight into preparation conditions for these materials by thermal treatments. To be able to reliably distinguish the different Pt-telluride phases and to identify phase mixtures also remains a challenge. Core-level photoemission spectroscopy is an important method to identify materials, particularly in thin film form. Using photoemission reliable reference data is a pre-requisite. Using synchrotron high-resolution photoemission spectra of the different phases, provides the reference data of the different Pt-Te phases that may be used by others to identify their materials. Finally, our studies demonstrate the excellent air stability of these materials with only weak adsorption at the very surface layer and no measurable oxidation. Air stability is critical to justify characterization of materials properties of air exposed samples, by e.g., transport measurements, and for further device fabrication. Thus, these studies suggest that the Pt-tellurides are suitable materials for further ex-vacuum investigations.

II. Methods

$PtTe_2$ samples are grown by MBE on graphite (HOPG) substrates at a growth temperature of 200 °C and at growth rate of ~ 1.3 monolayers per hour, similar to previous reports for MBE growth of $PtTe_2$ films.[12,16,19,21,22] The films were 4-5 $PtTe_2$ layers thick (~ 3nm) and the samples are characterized by STM and lab-source XPS before exposure to air and transport to the Elettra synchrotron in Trieste, Italy, where the samples have been characterized by high resolution XPS at the BACH beamline equipped with a Scienta R3000 hemispherical analyzer placed at an angle of 60° with respect to X-ray incidence direction. The incoming X-rays were linearly polarized with the polarization vector lying in the scattering plane. The samples were mounted on a ceramic heater made of pyrolytic boron nitride (PBN) with an embedded pyrolytic graphite (PG) layer. Temperature was measured by a thermocouple directly clamped to the surface of the sample. Binding energies were calibrated by measurement of the Fermi-edge of a Pt-foil mounted next to the sample. The total instrumental resolution was 0.25 eV and the XPS data were collected at normal emission geometry at a take-off angle of 90°. For the sample the Te-3d, Te-4d, Pt-4f core levels were monitored, in addition O-1s and C-1s core levels were monitored to gain insight in surface contamination and stability due to air exposure. The spectra were fitted with Voigt profiles, i.e. a convolution of Gaussian and Lorentzian line shapes, using the kolXPD software package.[23] Most studies were performed with a 700-eV photon energy, which allowed to monitor all core levels. At this photon energy the kinetic energy for the Te-3d is close to 120 eV and thus the photoemission spectrum is very surface sensitive. In contrast the photoemitted electrons from Pt-4f and Te-4d have a kinetic energy of 623 eV and 655 eV, respectively and thus have a probing depth of ~4 nm.[24] Samples were annealed by applying a linear temperature ramp of 1K/min while continuously monitoring the core levels. Acquiring a full set of core-levels during the temperature ramp takes around 270 seconds, so that a spectrum for each core level is obtained for a temperature change of 4.5 K. During heating, small shifts in the core levels can occur due to the applied potential on the heater especially at higher annealing temperatures (heater powers). At these higher temperatures the C-1s peak observed on our samples is coming from the graphite substrate and this provides a convenient reference to compensate for any heater induced peak shifts. Monitoring the core levels as a function of temperature enables determination of desorption of surface contaminants of air exposed samples and importantly the transformation of the initially $PtTe_2$ sample into different compositions by the loss of Te to the gas phase. In addition, other samples were also annealed to target temperatures that caused the transformation into specific compositions and high resolution XPS data were collected for these phases after cooling to room temperature. The chemical stability of the different Pt telluride compositions was assessed by exposure to air as well as to pure oxygen. Oxygen exposure was limited to a pressure of 10^{-6} mbar in the UHV chamber and up to 100 mbar in the attached load lock of the vacuum system. At either pressure the samples were exposed for 5 min to oxygen. Scanning tunneling microscopy measurements were taken at room temperature in constant current mode in UHV with the sample mounted by tantalum wires onto a flag-style sample plate.

III. Results and Discussions

A. Thermal stability and phase transformations

After cleaning the surface from surface adsorbates by annealing to ~ 200 ˚C (see discussion on air stability of the samples, below in section III.D), a constant temperature ramp was applied, and the core level spectra were recorded. Fig. 2 (a) and (b) shows the false-color intensity for the Te-4d and Pt-4f core levels, respectively, as a function of annealing temperature. From the intensity map it is apparent that

the Te-4d peak position is not changing much as function of temperature with only a small shift occurring at ~ 350 ˚C but some decrease in the peak intensity is observed as can be seen more clearly from the peak intensity versus temperature profile shown in Fig.2 (c). A discernable decrease in the intensity is observed between ~350-370 °C and 400-410 °C, before it drops more rapidly above 420 °C. A more detailed description of the core level binding energies will be given below. In contrast to Te-4d, the Pt-4f exhibits more pronounced shifts in the core level binding energies in addition to a change in their relative intensities. The intensity profile as function of temperature for binding energies of 72.5 eV, 71.6 eV, and 71.1 eV are plotted in Fig. 2 (d). As we show below, these binding energies correspond to the Pt-4f core levels in $PtTe_2$, Pt_2Te_2 and metallic Pt. In the temperature profile transitions in the intensity ratios of these components are observed at ~340-370 °C and ~390-415 °C, closely corresponding to the change in the intensity of the Te-4d peak. In between these temperature regions the Pt 4f intensities reach plateaus. Thus, the data indicates that the transformation from one phase to another occurs in certain temperature windows rather than a continuous transformation. The implication is that $PtTe_2$ is the least thermally stable phase, which transforms to Pt_3Te_4 above ~340 °C by loss of Te. Pt_3Te_4 is then stable to ~390 ˚C and transforms to Pt_2Te_2 which remains stable to ~415 °C when it starts to lose all Te and transforms to Pt-metal. Scanning tunneling microscopy (STM) measurement, shown in Fig. 3, of low temperature grown films that were subsequently vacuum annealed also confirm that these samples remain flat for all three phases. The STM images show that post growth annealing and transformation into different compositions even increases the size of atomically flat terraces. Maintaining a flat surface is critical for the post- growth annealing process to yield relevant thin film samples.

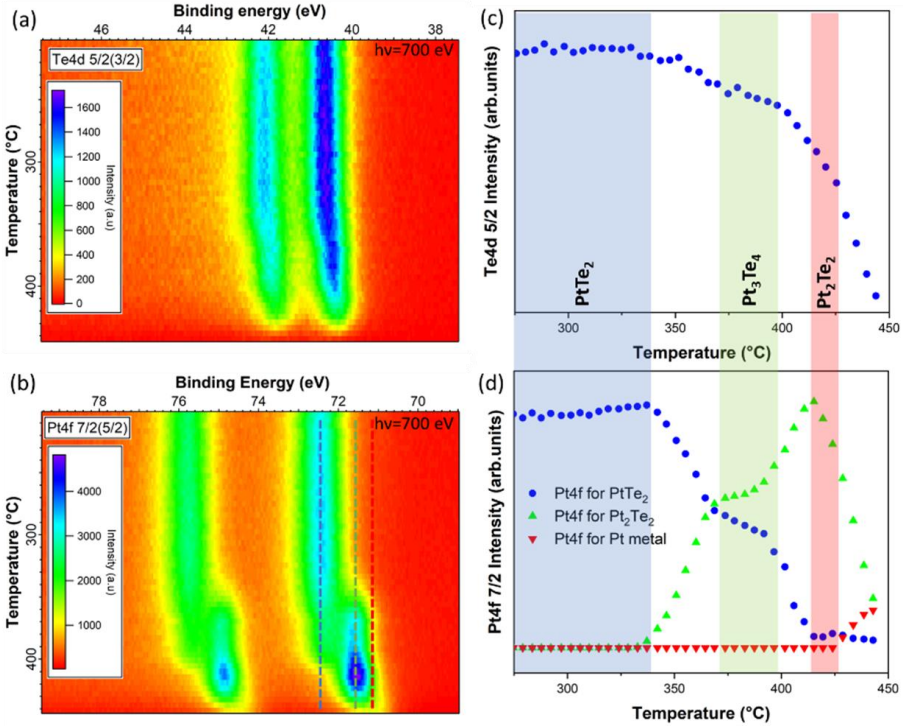

Figure 2: Temperature programmed photoemission for (a) Te 4d and (b) Pt 4f core levels. The peak intensity of $Te4d_{5/2}$ is shown in (c). For the Pt $4f_{7/2}$ three components are fitted with their binding energy indicated by the dashed lines in (b). The intensity of these components is plotted in (d), clearly showing the transitioning of one component to another. The color shaded areas in (c) and (d) indicate the temperature ranges in which only one phase is observed, i.e., the blue area is $PtTe_2$, the green area is Pt_3Te_4, and the red area is Pt_2Te_2.

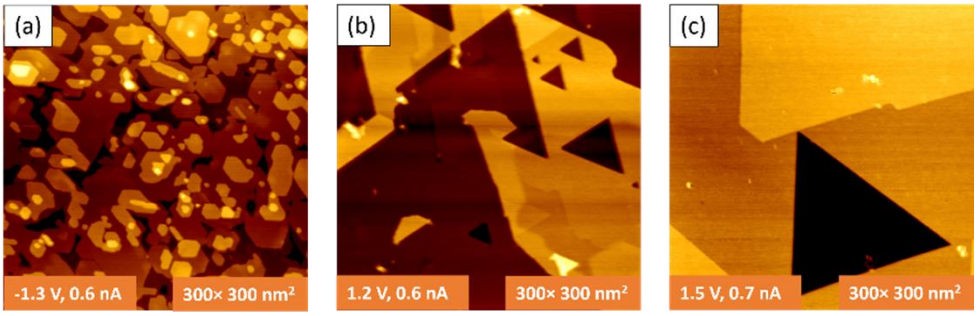

Figure 3: Large scale STM images of (a) as grown $PtTe_2$ sample, (b) after post-growth vacuum annealing induced transformation to Pt_3Te_4 and (c) after transformation to Pt_2Te_2. With increasing annealing, the atomically flat terraces become larger in size.

B. High resolution core level spectra of the different van der Waals Pt-telluride materials

To confirm and characterize the different phases in more detail a fresh sample is annealed to the corresponding target temperatures to create specific phases and the core level spectra are recorded. The samples were annealed at 280 °C, 365 °C, 405 °C for 20-30 min, which are below the first transition temperature, above the first transition, and above the second transition but before metallic Pt is observed, respectively. The Te-3d, Te-4d, and Pt-4f spectra for these three annealing temperatures are shown in Fig. 4. The Te-3d and Te-4d peaks can be fitted with a single doublet, while the Pt-4f may require 2 doublets. For the lowest annealing temperature, the sample is assigned to $PtTe_2$ but the shoulder on the low BE side suggests the presence of either a small amount of Pt_2Te_2 or adsorbed oxygen that has shown to also contribute to a Pt-4f shoulder at approximately the same binding energy and is discussed below in section D. Intermediate annealing temperatures cause a Pt_3Te_4 phase, and the last annealing creates a Pt_2Te_2 sample. All peaks can be fitted with a Voigt profile (Gaussian and Lorentzian convolution). The fitting parameters and core level binding energies for the three phases are summarized in Table 1. The Te-peak shape and BE for the three phases only change slightly indicating that Te remains in similar charge state. In contrast, Pt-4f exhibits pronounced changes in both BE and peak shape. Comparing $PtTe_2$ with Pt_2Te_2, The BE energy shifts by ~1.0 eV corresponding to a more positive charge state for Pt in $PtTe_2$. Pt in $PtTe_2$ has a significantly broader peak shape than in Pt_2Te_2. Since both peaks have negligible asymmetry and can be fit well by a Voigt profile the difference in the peak width should be related to different core-hole lifetimes.[25] The Pt_3Te_4 phase can be fit by a combination of two doublets with the line shapes for Pt_2Te_2 and $PtTe_2$, respectively. This agrees with the structure of Pt_3Te_4 that consists of alternating $PtTe_2$ and Pt_2Te_2 layers (see Fig. 1). However, a small shift in the BE of the $PtTe_2$ component is required to lower binding energy, compared to the pure $PtTe_2$ phase. This shift may indicate some electron transfer from the Pt_2Te_2 layers to the Pt in $PtTe_2$ layers and thus indicates that the electronic structure of $PtTe_2$ layers in Pt_3Te_4 is modified by the adjacent Pt_2Te_2 layers. Therefore, Pt_3Te_4 has unique properties and may not just be simply described as a mere combination of $PtTe_2$ and Pt_2Te_2.

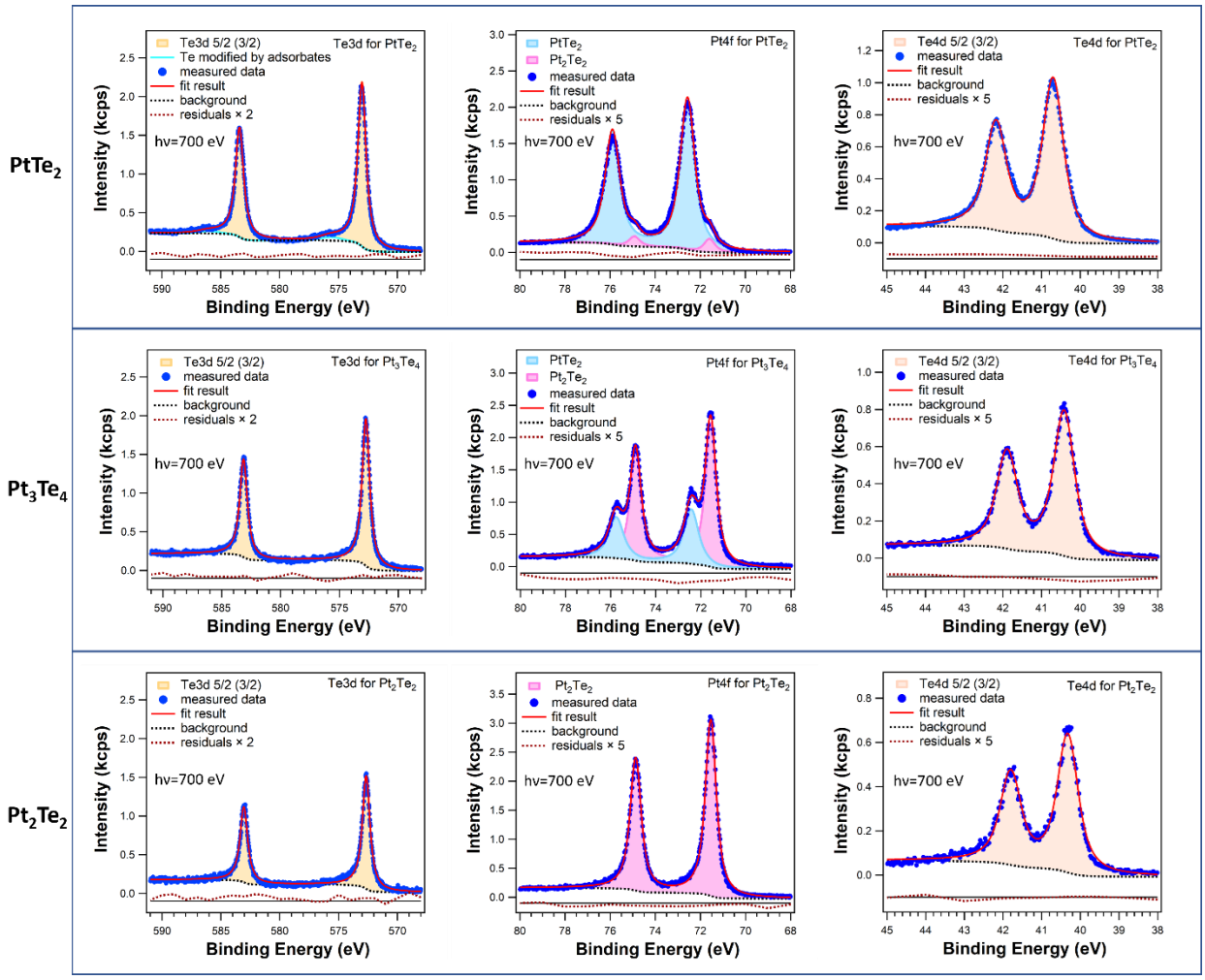

Figure 4: High resolution core level spectra for the three Pt-telluride phases.

Table 1: Fitting parameters for Pt-telluride phases.

	$PtTe_2$				Pt_3Te_4				Pt_2Te_2		
	Pt4f ($PtTe_2$)	Pt4f (Pt_2Te_2)	Te3d	Te4d	Pt4f ($PtTe_2$)	Pt4f (Pt_2Te_2)	Te3d	Te4d	Pt4f (Pt_2Te_2)	Te3d	Te4d
Lorentzian FWHM [eV]	0.63	0.49	0.82	0.49	0.63	0.49	0.75	0.49	0.49	0.75	0.49
Gaussian FWHM [eV]	0.32	0.24	0.16	0.31	0.32	0.24	0.16	0.31	0.24	0.16	0.31
Spin orbit split [eV]	3.33	3.33	10.4	1.48	3.33	3.33	10.4	1.48	3.33	10.4	1.48
Peak position [eV]	72.57	71.59	573	40.7	72.43	71.56	572.75	40.42	71.54	572.64	40.33
Peak area [kcps]	4.15	0.28	4.65	1.53	1.68	3.38	3.83	1.19	4.6	2.95	0.96
peak amplitude [kcps]	2.37	0.16	2.79	0.92	0.96	1.93	2.3	0.72	2.63	1.77	0.57

Finally, to further confirm the different phases the peak intensity ratios are assessed. For Pt_3Te_4 the two Pt components from the $PtTe_2$ and Pt_2Te_2 layers must have an intensity ratio of 1:2. With our peak fitting for the sample associated with this phase the peak ratio is 1:2.04, i.e., very close to the expected ratio and within the expected uncertainty of the peak fitting. Comparing the Pt:Te concentration ratio requires a more detailed analysis taking the elemental photoemission sensitivity at the used photon

energy into account. Moreover, the probing depth depends on the kinetic energy of the photoemitted electrons and thus only intensity ratios with similar kinetic energies can be compared. At 700 eV photon energy, Pt-4f and Te-4d have kinetic energies of 623.8 and 654.7 eV, respectively and thus similar probing depth. Moreover, the analyzer transmission function is constant over this small energy range.[26] The sensitive factors used for these core levels are 2.64 and 0.5, respectively, considering linearly polarized light and used measurement geometry.[27,28] Using the values of the peak areas shown in table 1, we thus estimate a Pt:Te ratio of 0.5, 0.8, 0.9 for the three samples. Small deviations from expected values may be a consequence of the layered structure and surface termination of the samples by Te, as well as the slightly larger escape depth (larger kinetic energy) for the Te-4d than Pt-4f photoelectrons.

C. Direct growth at different growth temperatures

The measured thermal stability and phase transformation by vacuum annealing raises the question if these three phases can be directly synthesized by controlling the growth temperature during MBE synthesis or a post growth vacuum annealing gives better phase control. Thus, we examined Pt-telluride film growth at three different substrate temperatures.

XPS measurements of samples grown at substrate temperatures of 200 ˚C, 390 ˚C, and 430 ˚C and at growth rate of ~ 1.3 monolayers per hour, are shown in Fig. 5. Here, the XPS measurements were acquired with a non-monochromatized Al K_α lab source, which naturally has a much lower resolution compared to the synchrotron studies. Nevertheless, the different phases can be identified from the Pt-4f peak fitting. As in the previous samples, $PtTe_2$ is obtained at low growth temperatures of 200 ˚C. However, we were not able to gain phase pure Pt_3Te_4 or Pt_2Te_2 samples by the direct growth method. Although with increasing growth temperature the Pt_2Te_2 fraction does increase, all the samples were a phase mixture and post-growth annealing is again required to transform these samples into pure phases. Thus, it appears that controlling the Pt-telluride phases in thin films by just controlling the substrate temperature during deposition is challenging. Instead, the post-growth vacuum annealing of $PtTe_2$ results in reproducible film stoichiometries and thus should be the preferred sample preparation for telluride films with low tellurium concentrations.

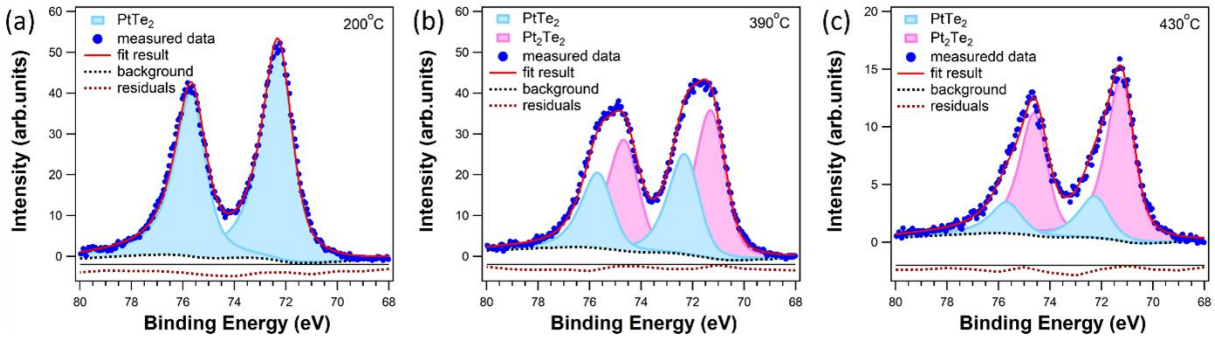

Figure 5: Pt-4f core levels of Pt-telluride films grown at three different substrate temperatures (a) 200 ˚C, (b) 390 ˚C, (c) 430 ˚C. With increasing substrate temperature, the Pt_2Te_2 component increases, but no phase pure materials have been reliably synthesized by varying the substrate temperature during growth. The spectra were acquired with a lab x-ray Al-K_α source and thus have lower resolution compared to the synchrotron data.

D. Air stability and thermal surface cleaning

In many applications air- and chemical- stability is a requirement for the materials to be suitable. This may be of particular importance for catalysis and electrocatalysis and for materials handling and processing in electronic device fabrication. We examined air-stability of $PtTe_2$. The sample was exposed to air for ~150h. After exposure to air, oxygen and carbon are detected by XPS on the $PtTe_2$ surface, as shown in Fig. 6, for the $PtTe_2$. Moreover, the Te-peak exhibits a broader second component at higher binding energies (Fig. 6). Comparing the more surface-sensitive Te-3d peak (kinetic energy ~ 120 eV) with the less surface- sensitive Te-4d (kinetic energy ~ 655 eV), it can be observed that the broad Te component is predominantly localized to the surface. This observation suggests that the high binding energy component can be attributed to Te surface atoms interacting with adsorbates. Annealing with a constant temperature ramp of 3 K/min reduces the carbon peak. The broad C-1s peak observed after air exposure becomes narrow at ~215 ˚C. This narrow peak is assigned to sp^2 carbon signal from the HOPG substrate. Thus at 215 ˚C most of the carbon contamination from the surface has desorbed or has been graphitized. In contrast the oxygen signal does not continuously decrease with annealing temperature. The O-1s signal initially increases before it decreases. A similar behavior is observed for the non-$PtTe_2$ Te-component at ~ 576 eV binding energy. This indicates that this Te-component is associated with adsorbed oxygen. The initial increase in both the O-1s as well as the Te-components can be explained by the desorption of carbon containing species and thus a decreased attenuation of the O-Te signal from the surface. At 280 ˚C the oxygen and Te-O signal have significantly decreased, indicating desorption of oxygen from the surface. In addition to the Te-O component, after air exposure the Pt-4f peak also exhibits an additional component at a similar binding energy to that of the Pt-4f peak of Pt_2Te_2 (see Fig. 6). However, the simultaneous decrease of this component with the O-1s and Te-O component indicates that this low binding energy component in Pt-4f is caused by the oxidation of surface Te which shifts the Pt peak to lower binding energy. This is a clear indication that oxygen interacts with Te and not with Pt since oxidation of Pt should cause a shift in the opposite direction.

A small oxygen signal, however, remains even after annealing to 280 ˚C. This oxygen signal is likely related to x-ray beam damage at the spot the sample was characterized. Moving away from this spot on the sample shows that a surface without oxygen is obtained and the Te component is that of pure $PtTe_2$. Thus, these studies demonstrate the extraordinary air stability of $PtTe_2$. While oxygen does chemisorb to the surface and form Te-O bonds that cause a Te-component at ~ 3 eV higher binding energy than the Te-component for $PtTe_2$, this oxygen can be desorbed from the surface by annealing to 280 ˚C.

The stability against oxidation is also established by exposing the clean $PtTe_2$ samples at up to 100 mbar static pressure of pure O_2 for 5 min at room temperature in the load lock of the UHV chamber. No significant differences are observed in the core level spectra after this procedure, as shown in Figure 7. This also indicates that oxygen is not easily activated at the $PtTe_2$ surface.

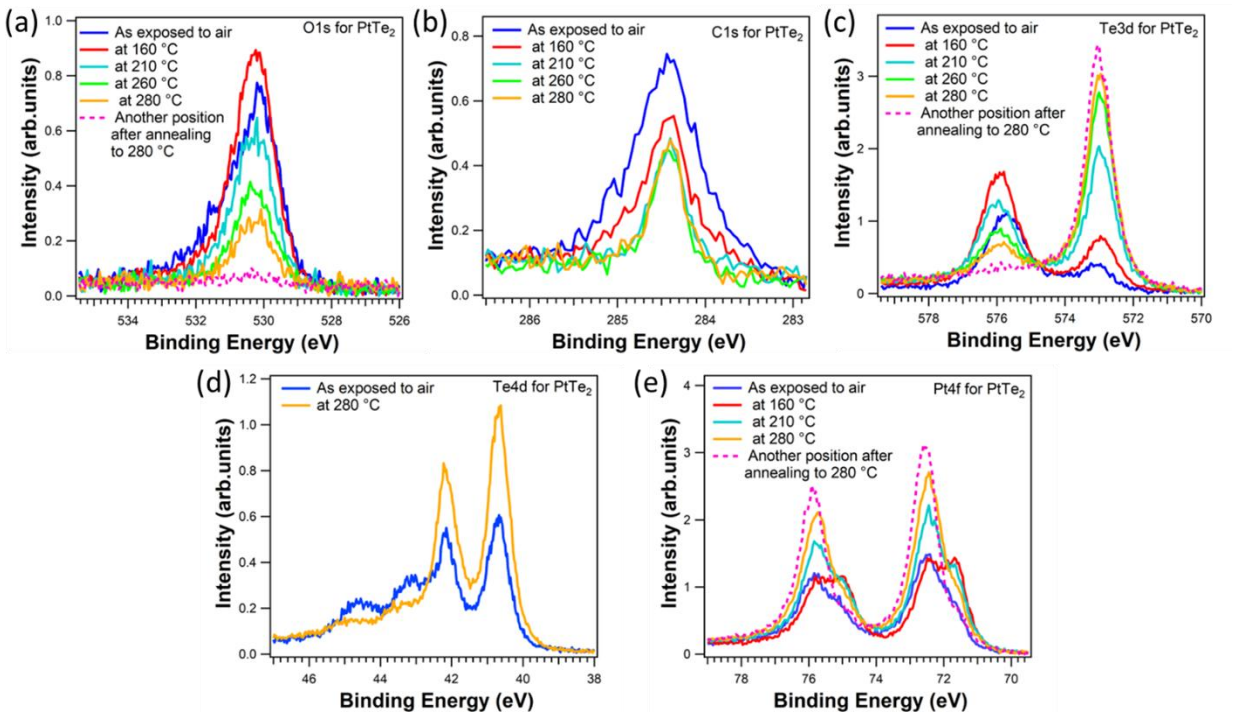

Figure 6: Core levels for a $PtTe_2$ sample after 150 h of air exposure and after subsequent vacuum annealing. The O-1s (a), C-1s (b), Te-3d (c), Te 4d (d), and Pt-4f (e) core levels are shown. The air exposure causes the surface Te to be modified and an additional Te-component shifted by ~ 3eV to higher binding energy is observed for both Te 3d and 4d core levels. The Pt-4f core level also shows modification after air exposure with a low binding energy component at a similar binding energy as for Pt_2Te_2. Annealing to 280 ˚C removes most oxygen and re-establishes the $PtTe_2$ core level component. Some beam induced oxidation remains and pristine surface without oxygen can only be found on the sample away from the beam, which is shown by the spectra indicated with a dashed line.

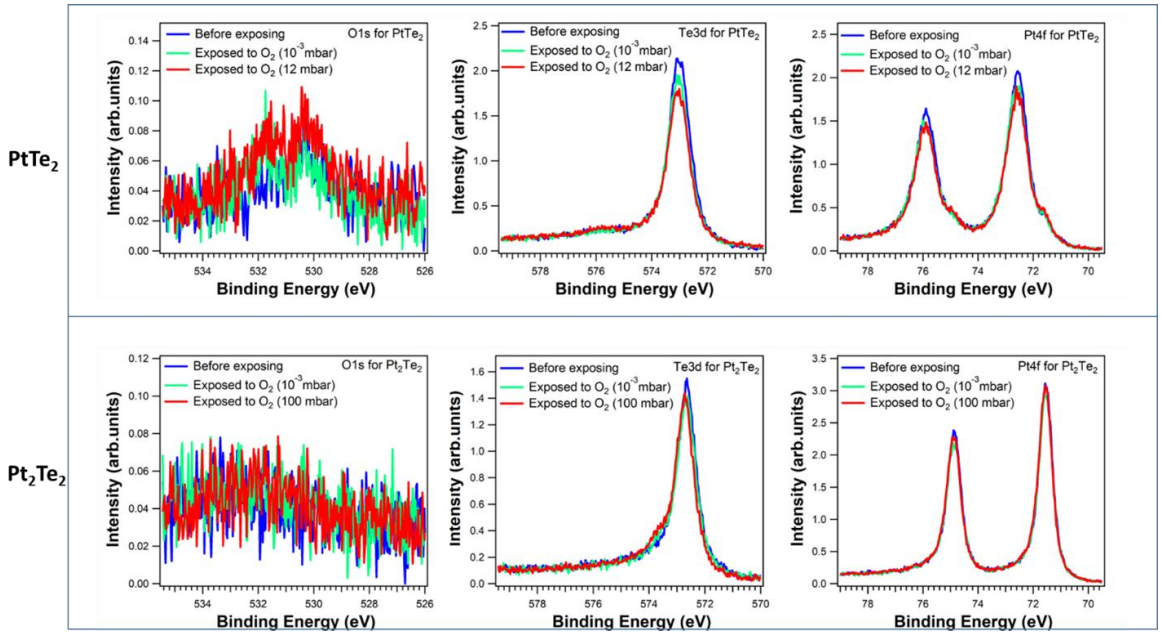

Figure 7: Core level spectra for $PtTe_2$ (top panel) and Pt_2Te_2 (bottom panel) before and after exposure to pure oxygen at 10^{-3}mbar and high pressures in the load lock (10 mbar for $PtTe_2$ and 100 mbar for Pt_2Te_2) with the sample at room temperature. For the Pt_2Te_2 sample oxygen exposure causes a weak shoulder on the high energy side of the Te-3$d_{5/2}$ peak.

In addition to $PtTe_2$ we also studied the air-stability of Pt_2Te_2. Samples transformed by vacuum annealing were taken out of the UHV chamber and stored in air for 15 h. The shorter air exposure time of Pt_2Te_2 compared to $PtTe_2$ limits the direct comparison of the two materials. After 15 h air exposure only small amounts of oxygen and carbon-species are observed on the Pt_2Te_2 surface, which are completely removed after annealing to 150 ˚C, as evident from the O-1s, C-1s and Te-3d spectra shown in Fig. 8. The C-1s peak can again be assigned to mainly signal from the HOPG substrate and the very surface sensitive Te-3d peak shows strong attenuation after air exposure from surface adsorbates but only a small intensity due to Te-O surface bonds, that disappear after annealing. This sample was also exposed to pure O_2 in the load lock which resulted in only a small high energy shoulder in the Te-3d core level (see Fig. 7) and no indication of oxygen adsorption. The shoulder may be associated with some chemical adsorption at defects sites on the surface. The lack of oxygen adsorption on Pt_2Te_2 by exposure at 100 mbar O_2 questions the theoretical claim that Pt_2Te_2 can activate oxygen for oxygen reduction electrocatalytic reactions,[10] however, further work under electrocatalytic conditions may be required.

The stability of the sample morphology by exposure to air can also be verified by STM studies. Fig. 9 shows an ultrathin $PtTe_2$ sample with $PtTe_2$ islands predominantly a single or two $PtTe_2$ molecular layers thick. After air exposure the surface cannot be imaged due to adsorbates. But after vacuum annealing to 250 ˚C the surface exhibits the same surface morphology as directly after growth. However, some adsorbate islands remain, which causes streakiness in the STM images at room temperature. The STM observations are generally in agreement with the photoemission which suggests an annealing to above 280 ˚C is required to remove most adsorbates.

Overall, these experiments demonstrate the excellent chemical stability of the Pt-tellurides which allows them to be removed from a vacuum growth chamber without significant degradation. Nevertheless, the

surfaces are going to be modified by adsorbates and these may affect defect induced properties on unprotected materials. The air stability does, however, suggest that the material after vacuum growth can be temporarily exposed to air for further processing and encapsulation for device applications. Applications in catalysis would need to be further tested under reactions conditions.

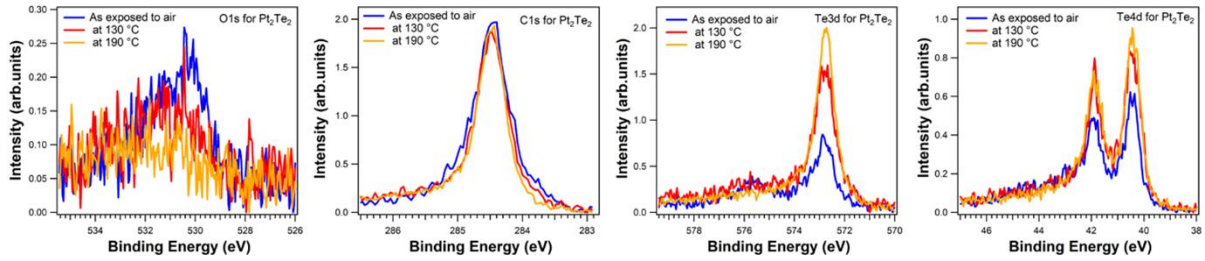

Figure 8: Core levels for a Pt_2Te_2 sample after 15 h of air exposure and after subsequent vacuum annealing. Only small amounts of O and corresponding small Te-$3d_{5/2}$ component at ~576 eV binding energy can be observed. After annealing to 190 ˚C the adsorbed oxygen is removed from the surface and spectra consistent with a pristine Pt_2Te_2 sample are obtained.

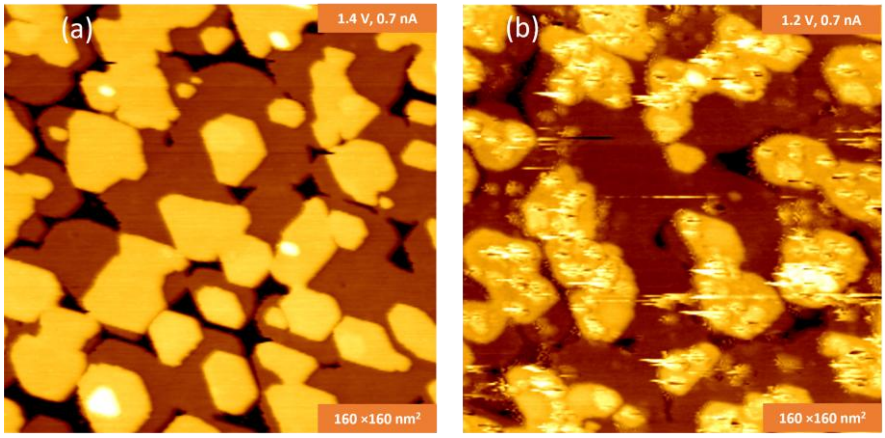

Figure 9: STM images of monolayer and bilayer $PtTe_2$ islands directly after growth (a) and after exposure to air for 24 h and subsequent vacuum annealing at 250 ˚C for 1h (b).

IV. Summary

In summary, we have shown that $PtTe_2$ films can be grown by MBE at low substrate temperatures. These films can be transformed in a controlled manner into Te-deficient phases of Pt_3Te_4 and Pt_2Te_2 by annealing in vacuum. $PtTe_2$ is stable up to ~ 330 ˚C before losing Te into the gas phase and the sample transforms into Pt_3Te_4. Pt_3Te_4 once formed is stable to 390 ˚C, when it starts losing Te and transforms to Pt_2Te_2. Above 420 ˚C the telluride completely decomposes, and metallic Pt is formed on the surface. This stepwise change in the sample composition allows the synthesis of different Pt-telluride van der Waals materials by controlled vacuum annealing. In contrast, direct growth at controlled substrate temperatures was not a reliable method for obtaining specific phases. The high-resolution synchrotron core level spectra for the different phases provide a reference for the binding energies for Pt-4f, Te-3d

and Te-4d core levels for the three different Pt-Te van der Waals phases. We also have demonstrated the air-stability of Pt-telluride. While prolonged exposure to air causes formation of Te-O bonds at the surface, that is evident by a ~3 eV binding energy shift of the surface Te atoms, the surface oxygen can be desorbed by vacuum annealing to ~ 280 ˚C and a pristine sample can be re-established. This demonstrates a resistance to oxidation of the sample, but chemisorbed oxygen at the surface in non-vacuum characterization of these materials must be considered.

Acknowledgment: Financial support from the National Science Foundation under award 2140038 is acknowledged. We acknowledge Elettra Sincrotrone Trieste for providing access to its synchrotron radiation facilities. I.P. and F.B. acknowledge funding from EUROFEL project (RoadMap Esfri).

References:

[1] C. Guo, L. Huang, C. Li, S. Shang, Z. Du. Thermodynamic modeling of the Pt-Te and Pt-Sb-Te systems, J. Electr. Mater. **44**, 2638 (2015).

[2] W.-S. Kim, Re-investigation of the phase constitution of the system Pt-Te, Metals Mater. **2**, 9 (1996).

[3] K. Cenzual, L.M. Gelato, M. Penzo, E. Parthé, Overlooked triagonal symmetry in structures reported with monoclinic centered Bravais lattices, trigonal description of Li_8Pb_3, PtTe, Pt_3Te_4, Pt_2Te_3, $LiFe_6Ge_4$, $LiFe_6Ge_5$, $CaGa_6Te_{10}$, and $La_{3.266}Mn_{1.1}S_6$, Zeitschr. Kristallogra **193**, 217 (1990).

[4] S. Kirklin, J.E. Saal, B. Meredig, A. Thompson, J.W. Doak, M. Aykol, S. Rühl, C. Wolverton, The Open Quantum Materials Database (OQMD): Assessing the accuracy of DFT formation energies. npj Comp. Mater. **1**, 15010 (2015).

[5] V.V. Subbotin, A. Vymazalová, F. Laufek, Y.E. Savchenko, C.J. Stanley, D.A. Gabov, J. Plášil. Mitrofanovite, Pt_3Te_4, a new mineral from the East Chuarvy deposit, Fedorovo–Pana intrusion, Kola Peninsula, Russia, Mineral. Mag. **83**, 523 (2019).

[6] N.F. Rosli, C.C. Mayorga-Martinez, N.M. Latiff, N. Rohaizad, Z. Sofer, A.C. Fisher, M. Pumera, Layered $PtTe_2$ matches electrocatalytic performance of Pt/C for oxygen reduction reaction with significantly lower toxicity. ACS Sustain. Chem. Eng. **6**, 7432 (2018).

[7] X. Chia, A. Adriano, P. Lazar, Z. Sofer, J. Luxa, M. Pumera, Layered platinum dichalcogenides (PtS_2, $PtSe_2$, and $PtTe_2$) electrocatalysis: Monotonic dependence on the chalcogen size, Adv. Funct. Mater. **26**, 4306 (2016).

[8] H. Huang, X. Fan, D.J. Singh, W. Zheng, Modulation of hydrogen evolution catalytic activity of basal plane in monolayer platinum and palladium dichalcogenides. ACS Omega **3**, 10058 (2018).

[9] D.W. Boukhvalov, J. Cheng, G. D'Olimpio, F.C. Bocquet, C.-N. Kuo, A.B. Sarkar, B. Ghosh, I. Vobornik, J. Fujii, K. Hsu, L.-M. Wang, O. Azulay, G.N. Daptary, D. Naveh, C.S. Lue, M. Vorokhta, A. Agarwal, L. Zhang, A. Politano. Unveiling the mechanisms ruling the efficient hydrogen evolution reaction with Mitrofanovite Pt_3Te_4, J. Phys. Chem. Lett. **12**, 8627 (2021).

[10] Y. Wang, Y. Li, T. Heine, PtTe monolayer: Two-dimensional electrocatalyst with high basal plane activity toward oxygen reduction reaction. J. Am. Chem. Soc. **140**, 12732 (2018).

[11] J. Fujii, B. Ghosh, I. Vobornik, A.B. Sarkar, D. Mondal, C.-N. Kuo, F.C. Bocquet, L. Zhang, D.W. Boukhvalov, C.S. Lue, A. Agarwal, A. Politano. Mitrofanovite Pt_3Te_4: A topological metal with termination-dependent surface band structure and strong spin polarization. ACS Nano. **15**, 14786 (2021).

[12] M. Yan, H. Huang, K. Zhang, E. Wang, W. Yao, K. Deng, G. Wan, H. Zhang, M. Arita, H. Yang, Z. Sun, H. Yao, Y. Wu, S. Fan, W. Duan, S. Zhou, Lorentz-violating type-II Dirac Fermions in transition metal dichalcogenide $PtTe_2$. Nat. Commun. **8**, 257 (2017).

[13] H. Xu, J. Wei, H. Zhou, J. Feng, T. Xu, H. Du, C. He, Y. Huang, J. Zhang, Y. Liu, H.-C. Wu, C. Guo, X. Wang, Y. Guang, H. Wei, Y. Peng, W. Jiang, G. Yu, X. Han, High spin Hall conductivity in large-area yype-II Dirac semimetal $PtTe_2$. Adv. Mater. **32**, 2000513 (2020).

[14] K. Deng, M. Yan, C.-P. Yu, J. Li, X. Zhou, K. Zhang, Y. Zhao, K. Miyamoto, T. Okuda, W. Duan, Y. Wu, X. Zhong, S. Zhou, Crossover from 2D metal to 3D Dirac semimetal in metallic $PtTe_2$ films with local Rashba effect. Sci. Bull. **64**, 1044 (2019).

[15] K. Zhang, M. Wang, X. Zhou, Y. Wang, S. Shen, K. Deng, H. Peng, J. Li, X. Lai, L. Zhang, Y. Wu, W. Duan, P. Yu, S. Zhou, Growth of large acale PtTe, $PtTe_2$ and $PtSe_2$ films on a wide range of substrates. Nano Research **14**, 1663 (2021).

[16] J. Li, M. Ghorbani-Asl, K. Lasek, V. Pathirage, A.V. Krasheninnikov, M. Batzill, A van der Waals heterostructure with an electronically textured moiré pattern: $PtSe_2/PtTe_2$. ACS Nano **17**, 5913 (2023).

[17] J. Li, S. Kolekar, M. Ghorbani-Asl, T. Lehnert, J. Biskupek, U. Kaiser, A.V. Krasheninnikov, M. Batzill Layer-dependent band gaps of platinum dichalcogenides. ACS Nano **15**, 13249 (2021).

[18] K. Lasek, J. Li, M. Ghorbani-Asl, S. Khatun, O. Alanwoko, V. Pathirage, A.V. Krasheninnikov, M. Batzill, Formation of in-plane semiconductor–metal contacts in 2D platinum telluride by converting $PtTe_2$ to Pt_2Te_2. Nano Lett. **22**, 9571 (2022).

[19] J. Li, S. Kolekar, Y. Xin, P.M. Coelho, K. Lasek, F.A. Nugera, H.R. Gutierrez, M. Batzill. Thermal phase control of two-dimensional Pt-chalcogenide (Se and Te) ultrathin epitaxial films and nanocrystals. Chem. Mater. **33**, 8018 (2021).

[20] K. Lasek, M. Ghorbani-Asl, V. Pathirage, A.V. Krasheninnikov, M. Batzill. Controlling stoichiometry in ultrathin van der Waals Films: $PtTe_2$, Pt_2Te_3, Pt_3Te_4, and Pt_2Te_2, ACS Nano **16**, 9908 (2022).

[21] L. Zhang, T. Yang, Arramel, Y.P. Feng, A.T.S. Wee, Z. Wang, MBE-grown ultrathin $PtTe_2$ film and the layer-dependent electronic structure. Nanoscale **14**, 7650 (2022).

[22] M.-K. Lin, R.A.B. Villaos, J.A. Hlevyack, P. Chen, R.-Y. Liu, C.-H. Hsu, J. Avila, S.-K. Mo, F.-C. Chuang, T.C. Chiang, Dimensionality-mediated semimetal-semiconductor transition in ultrathin $PtTe_2$ films. Phys. Rev. Lett. **124**, 036402 (2020).

[23] https://www.elettra.eu/lightsources/elettra/elettra-beamlines/msb/software-kolxpd.html

[24] M.P. Seah, W.A. Dench, Quantitative electron spectroscopy of surfaces: A standard data base for electron inelastic mean free paths in solids. Surf. Interf. Analysis 1, 2-11 (1979).

[25] C.R. O'Connor, M.A. van Spronsen, M. Karatok, J. Boscoboinik, C.M. Friend, M.M. Montemore. Predicting x-ray photoelectron peak shapes: The effect of electronic structure. J. Phys. Chem. C **125**, 10685 (2021).

[26] G. Drera, G. Salvinelli, J. Åhlund, P.G. Karlsson, B. Wannberg, E. Magnano, S. Nappini, L. Sangaletti. Transmission function calibration of an angular resolved analyzer for X-ray photoemission spectroscopy: Theory vs experiment. J. Elect. Spec. Rel. Phenom. **195**, 109-116 (2014).

[27] J.J. Yeh, Atomic Calculation of Photoionization Cross-Sections and Asymmetry Parameters, Gordon and Breach Science Publishers, Langhorne, PE (USA), 1993.

[28] J.J. Yeh, I. Lindau, Atomic subshell photoionization cross sections and asymmetry parameters: $1 \leqslant Z \leqslant 103$, Atomic Data and Nuclear Data Tables **32**, 1 (1985).